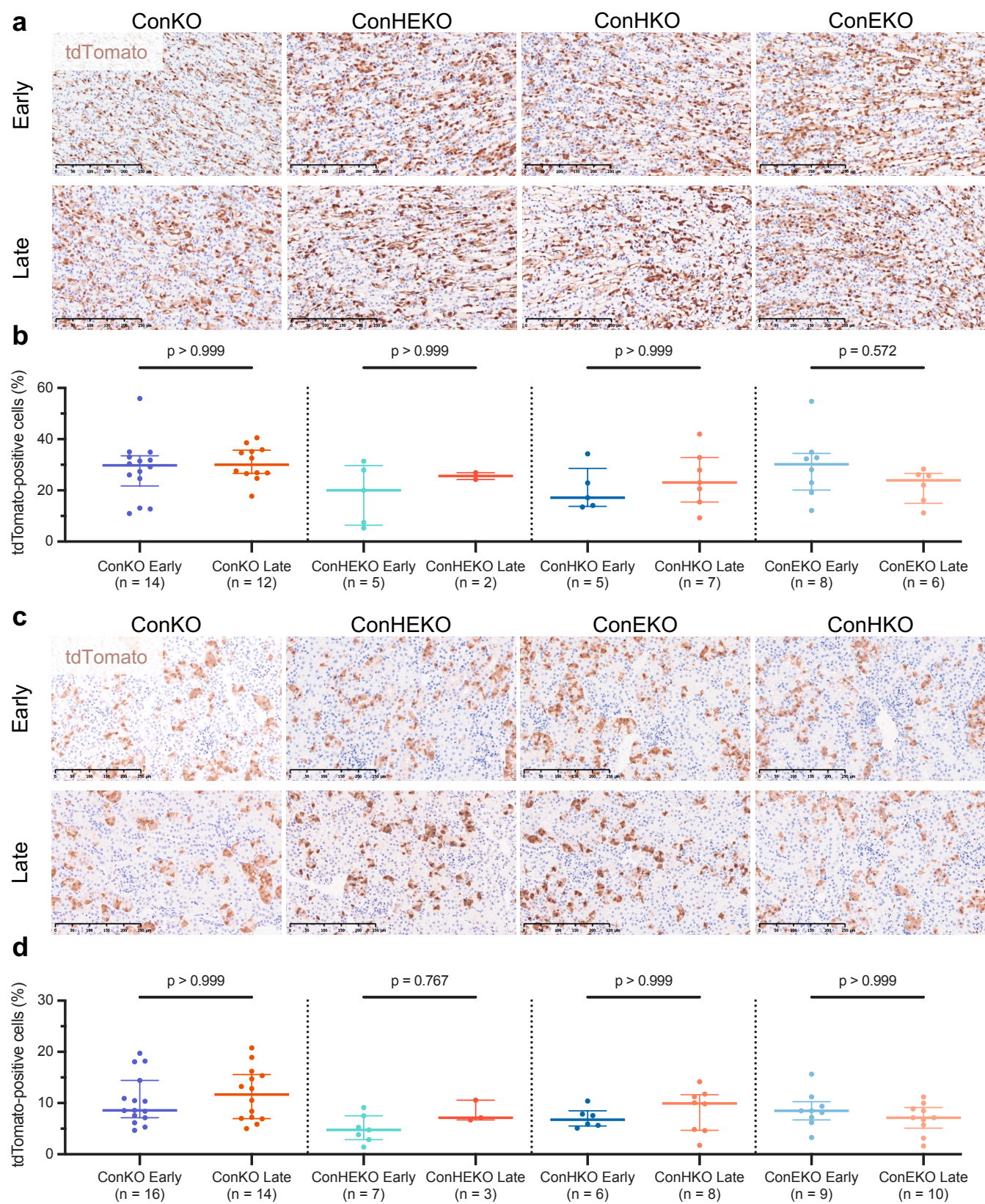


**Supplementary Fig. 1: Co-deletion of *Hif1a* and *Epas1* in tdTomato-tagged *Vhl*-recombined cells.**

**(a)** Schematic diagram depicting the design and recombination of the *Vhl<sup>lpr.fl</sup>* allele. *Vhl<sup>lpr.fl</sup>* and *Vhl<sup>lpr.KO</sup>* refer to ‘floxed’ and ‘knockout’ forms of the *Vhl<sup>lpr</sup>* allele. P, *Vhl* promoter; U, untranslated region; E, *Vhl* exon; I, *Vhl* intron; pA, polyadenylation site; P2A, porcine teschovirus 2A peptide; SA, splice acceptor. Dashed lines - spliced and translated regions; lightning symbols - excitation and emission wavelengths for tdTomato fluorescence. Red crossed circle indicates no interaction between VHL exon 1 fragment and HIF $\alpha$  or Elongin B/C. **(b)** *Vhl* allele construction for ConKO and VKO mice. Mice of both genotypes carry the *Vhl<sup>lpr.fl</sup>* allele. ConKO mice carry a second wild-type *Vhl<sup>wt</sup>* allele, while VKO mice carry a constitutively inactivated *Vhl<sup>lpr.KO</sup>* allele. **(c)** Genomic PCR for *Hif1a* and *Epas1* alleles performed on FAC-sorted tdTomato-positive cells from VHKO, VEKO, and VHEKO mice given 5x 2 mg tamoxifen and harvested early (1-3 weeks) after recombination. Expected amplicon sizes for wild-type (wt), floxed/unrecombined (fl) and knock-out/recombined (KO) forms of *Hif1a* and *Epas1* depicted by black arrows.

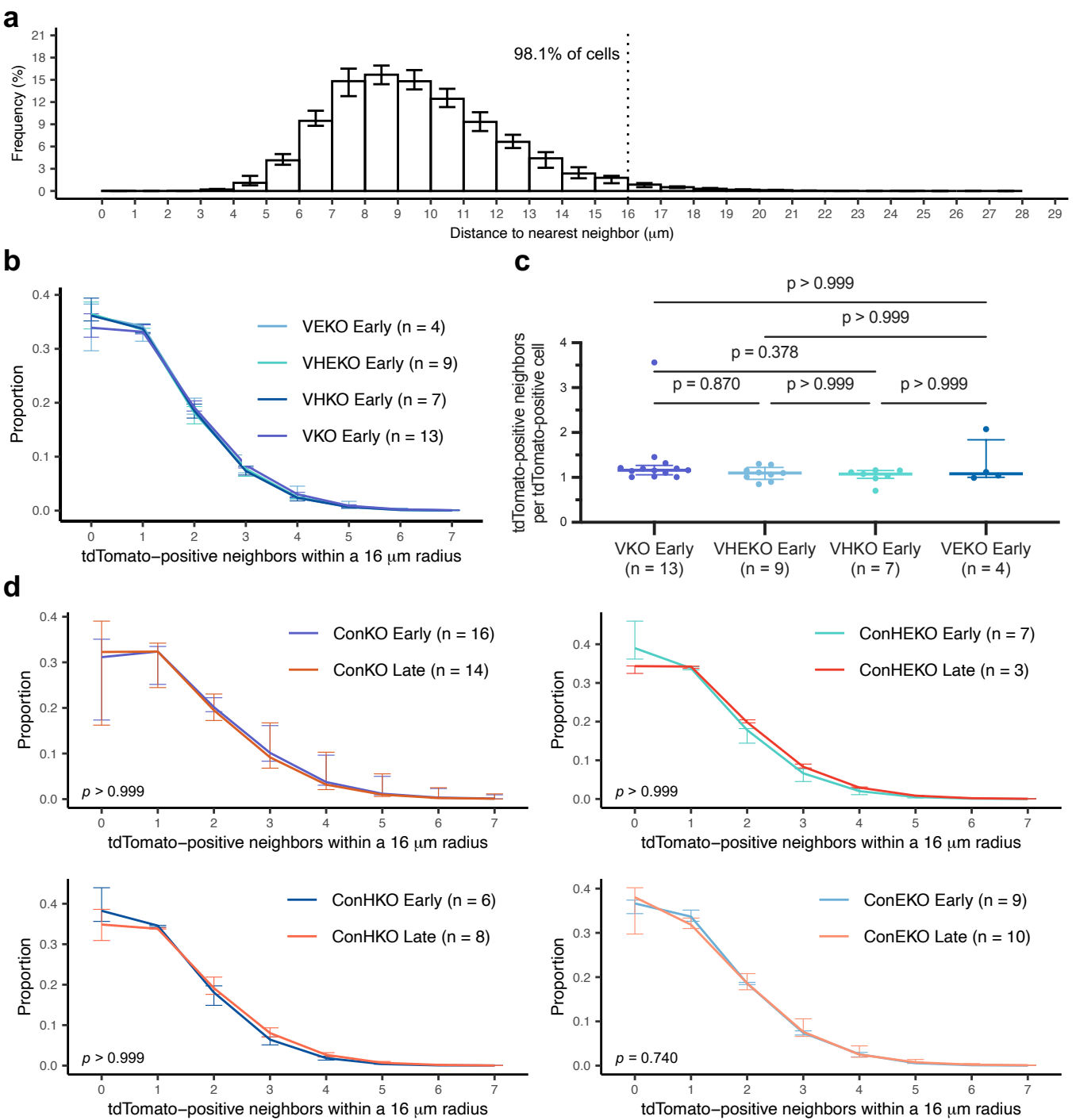




**Supplementary Fig. 2: Response to HIF $\alpha$  inactivation in different renal regions of ‘control’ kidneys.**

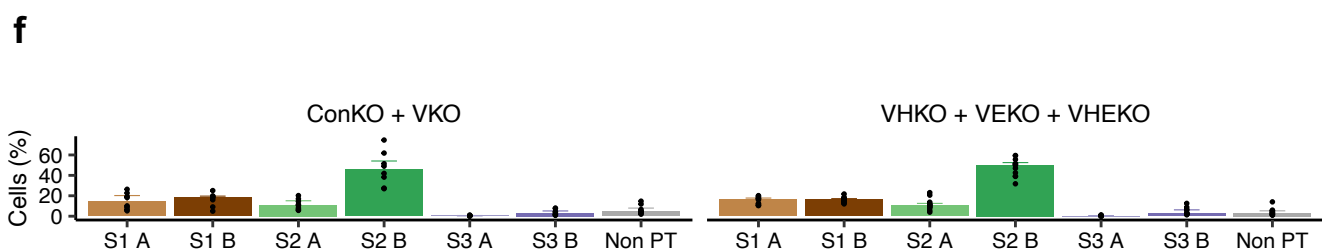
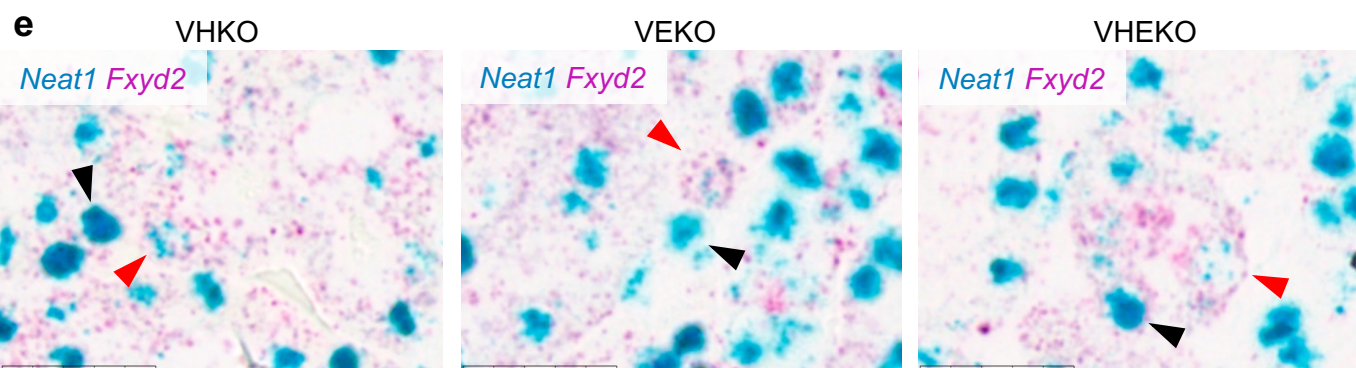
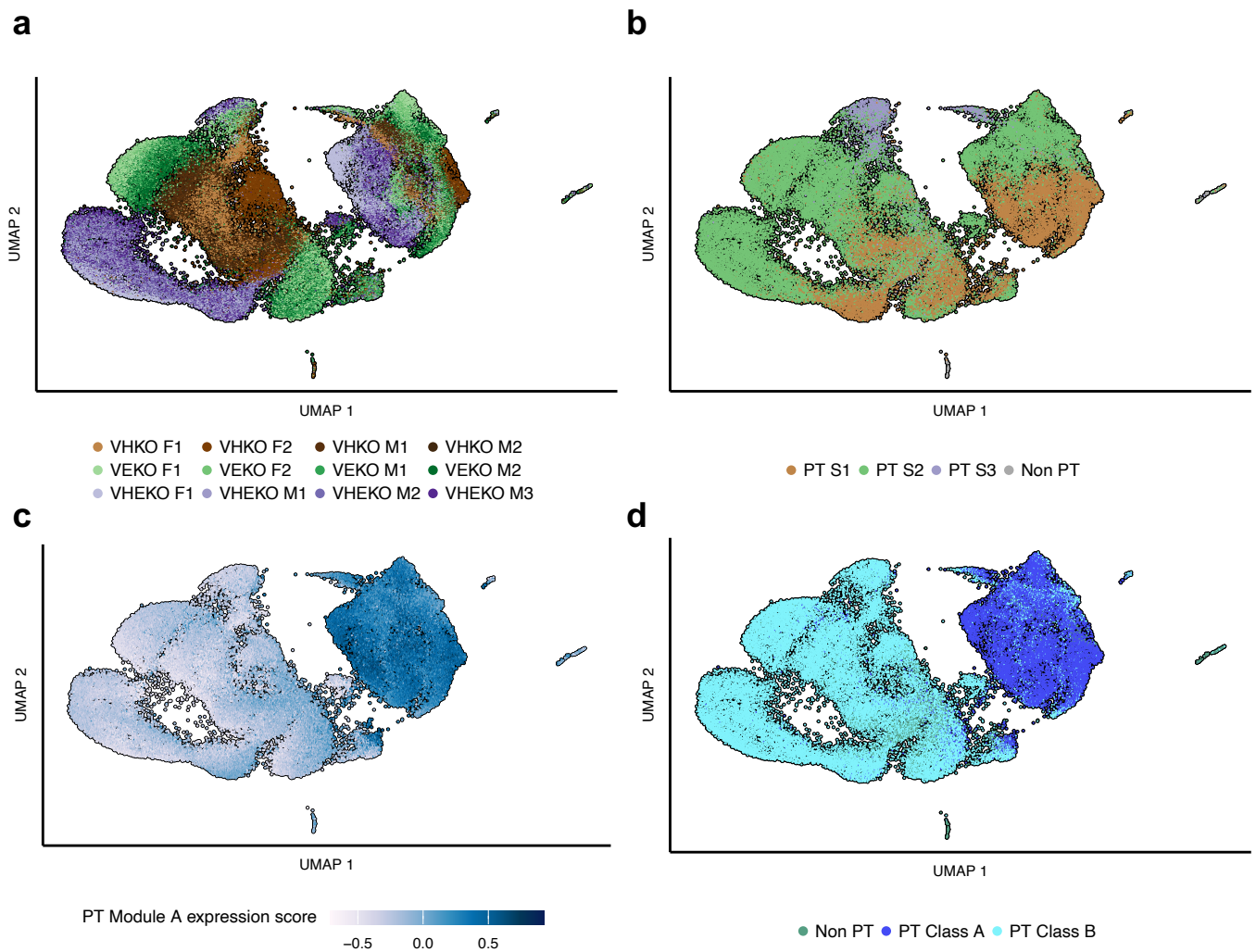
**(a, c)** Representative tdTomato IHC counterstained with hematoxylin in the renal papilla **(a)** or renal cortex and outer medulla **(c)** of ConKO, ConHKO, ConEKO, and ConHEKO mice given 5x 2 mg tamoxifen and harvested early (1-3 weeks) or late (4-12 months) following recombination. Scale bar denotes 250  $\mu$ m; 20x magnification.

**(b, d)** Automated quantification (see **Methods**) of the proportion of cells that are tdTomato-positive in the renal papilla **(b)** or renal cortex and outer medulla **(d)**. Pairwise comparisons by Kruskal-Wallis test with Dunn’s correction. Data are presented as median values, with the inter-quartile range indicated by error bars.



**Supplementary Fig. 3: Spatial distribution of cells in the renal cortex and outer medulla.**

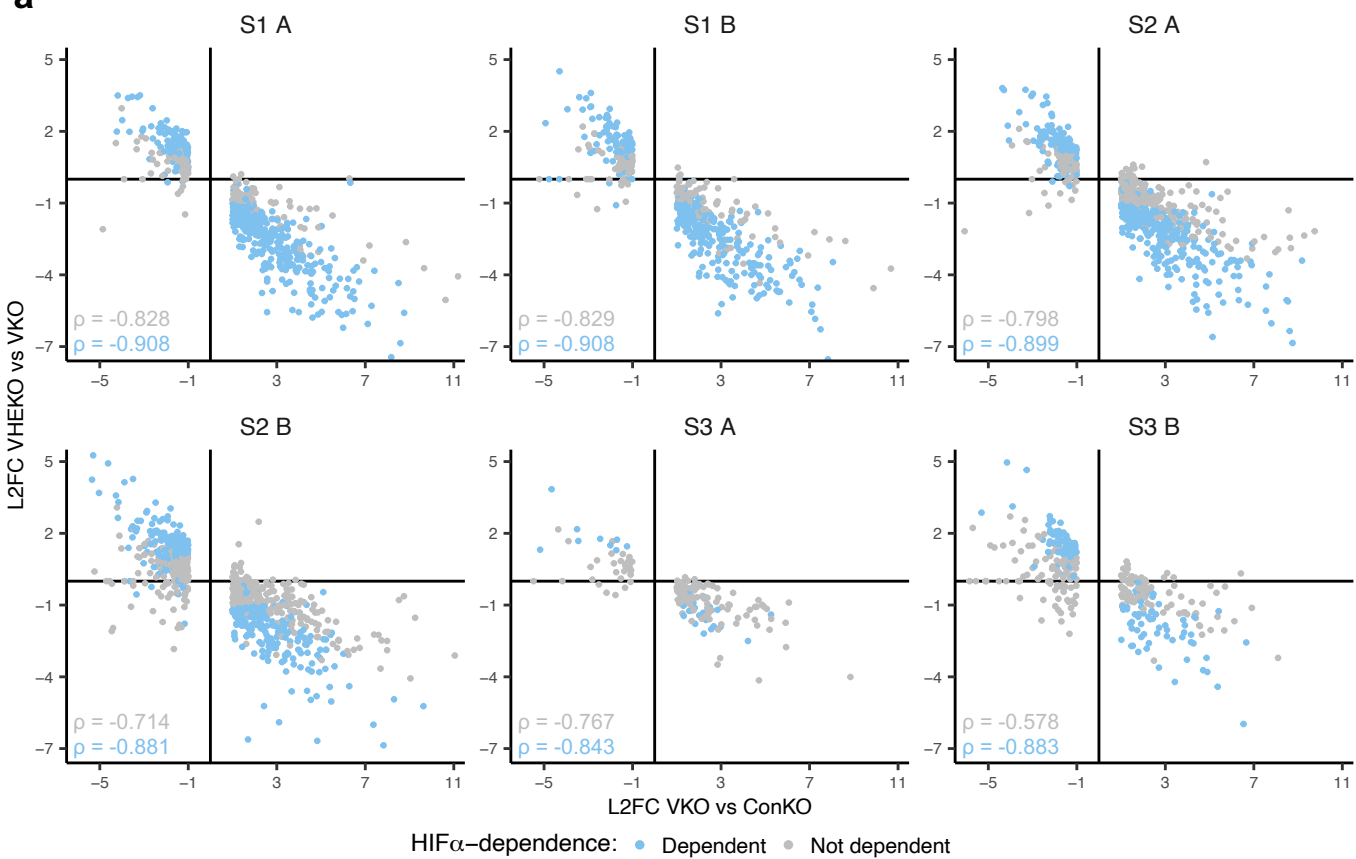
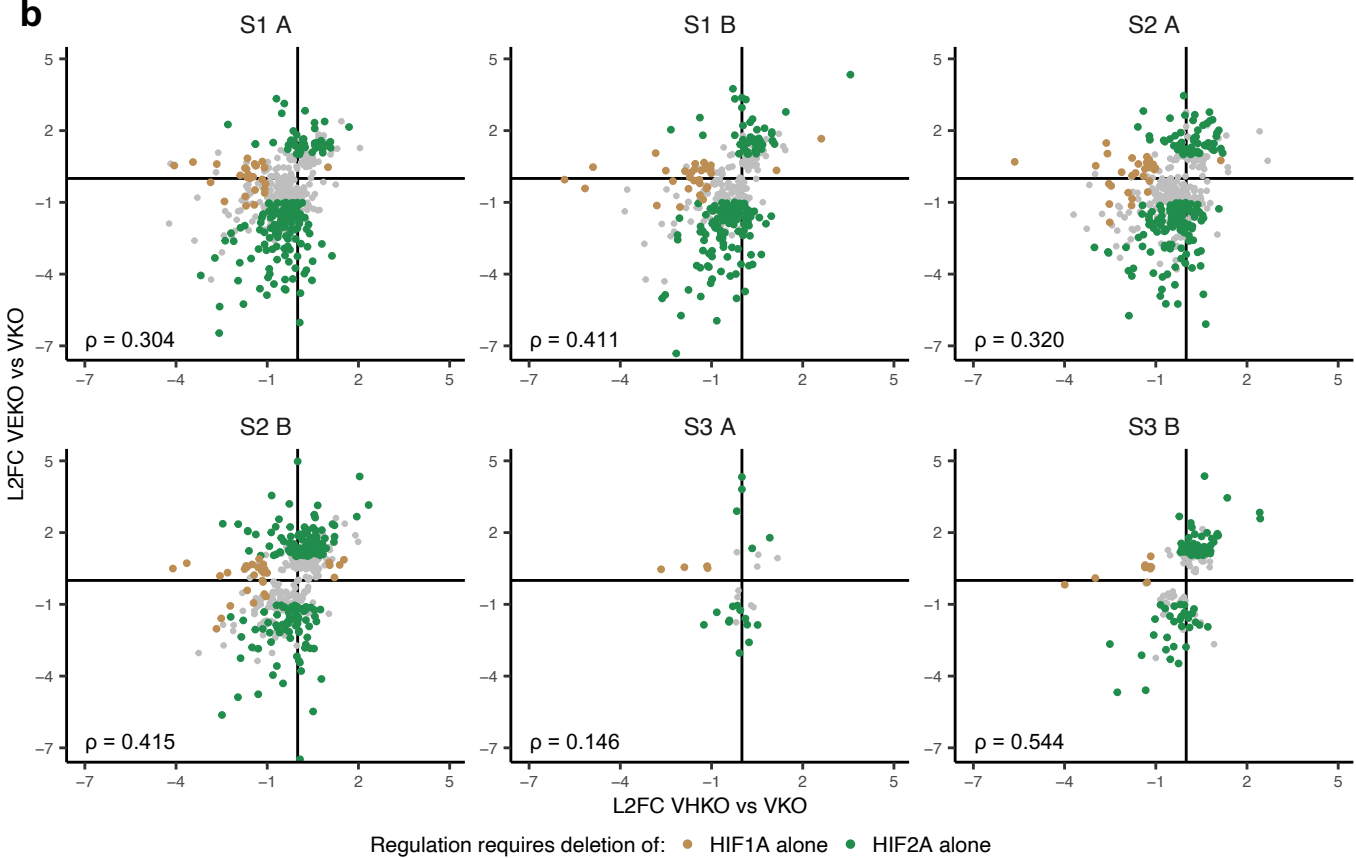
**(a)** Histogram depicting the distance to the nearest neighbor, whether tagged or untagged, for tdTomato-positive cells in the renal cortex and outer medulla. Median and interquartile range indicated. 50,000 cells analyzed over  $n = 10$  mice chosen randomly across all genotypes and timepoints. **(b, c)** Frequency distribution **(b)**, and mean number **(c)** of tdTomato-positive neighbors of tdTomato-positive cells within a 16  $\mu\text{m}$  radius in the cortex and outer medulla of VKO, VHEKO, VHKO, and VEKO mice harvested early (1-3 weeks) after *Vhl* inactivation. Data are presented as median values, with the inter-quartile range indicated by error bars. Pairwise comparisons by Kruskal-Wallis test with Dunn's correction. **(d)** Frequency distribution of tdTomato-positive neighbors of tdTomato-positive cells within a 16  $\mu\text{m}$  radius in the cortex and outer medulla of ConKO, ConHEKO, ConHKO, and ConEKO mice harvested either early or late after *Vhl* inactivation. Frequency distributions compared using Wilk's lambda statistic in multivariate analysis of variance (MANOVA).





**Supplementary Fig. 4: Single-cell RNA sequencing of tdTomato-tagged cells from VHKO, VEKO, and VHEKO mice.**

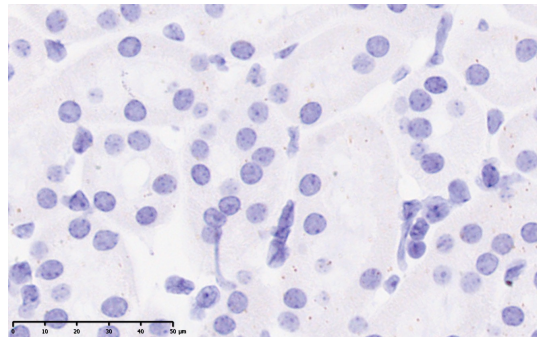
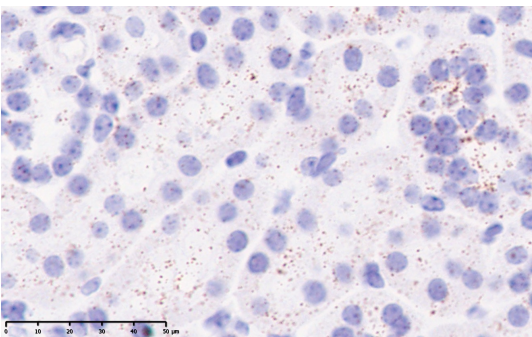
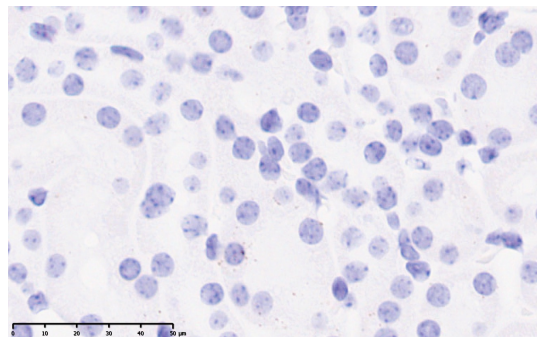
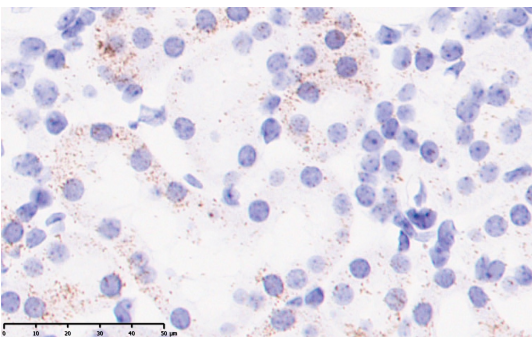
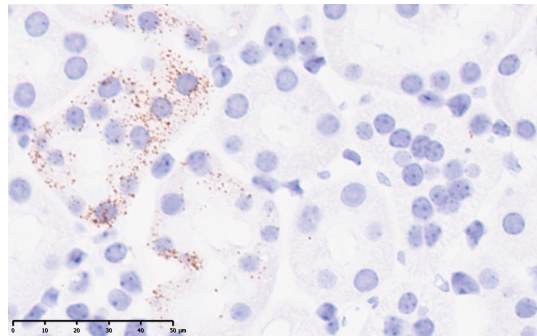
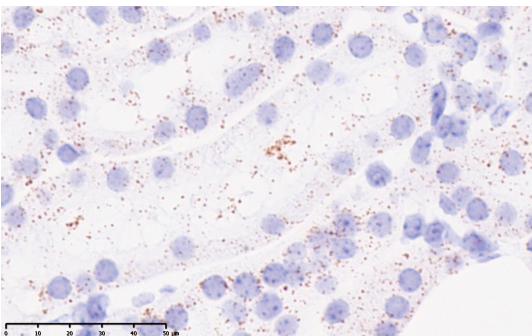
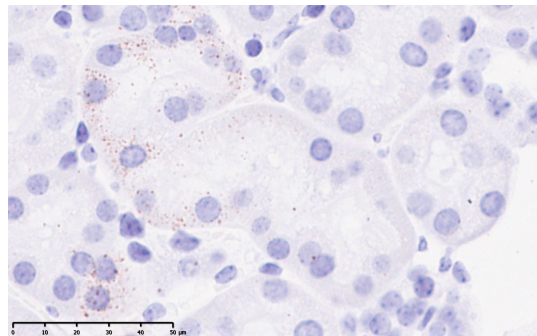
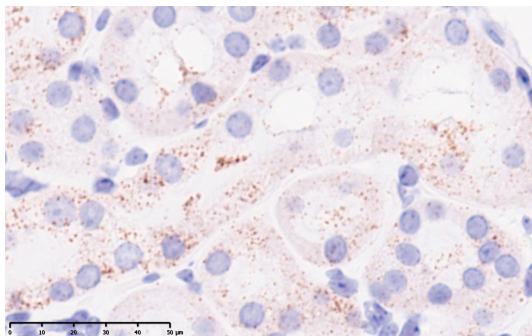
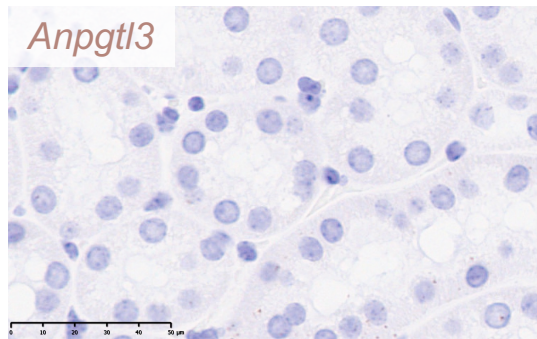
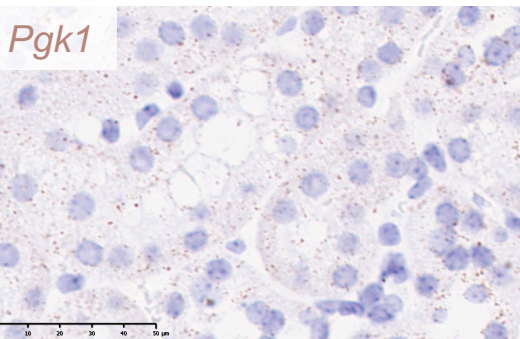
**(a-d)** UMAP plots depicting tdTomato-positive cells of n = 4 VHKO, VEKO, and VHEKO mice harvested at 4-12 months following *Vhl* and *Hif1a* and/or *Epas1* inactivation. **(a)** Data distribution by individual mouse. Cell colors are shaded according to the individual mouse within the genotypic group (VHKO in shades of brown; VEKO in shades of green; VHEKO in shades of purple). M = Male; F = Female. Concordance of the shades of the colors in UMAP space illustrates the reproducibility of the data. **(b)** Data distribution by assigned renal cell type. Proximal Tubule (PT). Cells of the same cell type are positioned together in UMAP space. **(c)** Expression score for PT Module A. High and low expression of PT Module A associates with distinct areas in UMAP space. **(d)** Data distribution by PT class as defined by PT Module A expression score. **(e)** Representative dual RNA *in situ* hybridization for *Neat1* (blue) and *Fxyd2* (pink) mRNA in kidney sections from VHKO, VEKO, and VHEKO mice. PT Class A (*Neat1*<sup>high</sup>/*Fxyd2*<sup>low</sup>; black arrows) and PT Class B (*Neat1*<sup>low</sup>/*Fxyd2*<sup>high</sup>; red arrows) cells are indicated. **(f)** Proportion of cells (median and inter-quartile range) that are of each PT identity in scRNA-seq datasets of ConKO and VKO (left), or VHKO, VEKO, and VHEKO (right) cells. Both datasets exhibit similar composition of PT identities. **(b, d)** All cell types other than PT S1, S2, and S3 cell types are assigned as ‘Non PT’.

**a****b**

**Supplementary Fig. 5: HIF $\alpha$  isoform-specific dependence of gene expression in *Vhl*-null cells.**

**(a)** Effects of combined *Hif1a* and *Epas1* deletion on expression of *Vhl*-dependent genes in each PT identity. Each scatter plot depicts pseudo-bulked log<sub>2</sub>-fold changes (L2FC) for *Vhl*-dependent genes in VHEKO *versus* VKO mice (HIF $\alpha$ -dependence) plotted against the changes in VKO *versus* ConKO mice (*Vhl* dependence) harvested late after recombination. Genes defined as significantly regulated by HIF $\alpha$  co-deletion (blue) and those whose alteration was not significant (grey). Spearman correlation coefficients ( $\rho$ ) provided separately for genes defined (blue) or not defined (grey) as significantly HIF $\alpha$ -dependent. Note that both significant and non-significant regulation by HIF $\alpha$  is anti-correlated with regulation by *Vhl*. **(b)** Isoform-specific effects of *Hif1a* and *Epas1* deletion on *Vhl*-dependent genes in each PT identity. Each scatter plot depicts pseudo-bulked L2FC for *Vhl*-dependent genes in VHEKO *versus* VKO mice (HIF1A-dependence) plotted against the changes in VHEKO *versus* VKO mice (HIF2A-dependence) harvested late after recombination. Spearman correlation coefficient ( $\rho$ ). Note that regulation by HIF1A is not strongly correlated with regulation by HIF2A. Genes whose regulation was reversed significantly by individual deletion of *Hif1a* but not *Epas1* ('HIF1A alone'; brown) and by *Epas1* but not *Hif1a* ('HIF2A alone'; green). Other HIF $\alpha$ -dependent genes (grey).





ConKO

VKO

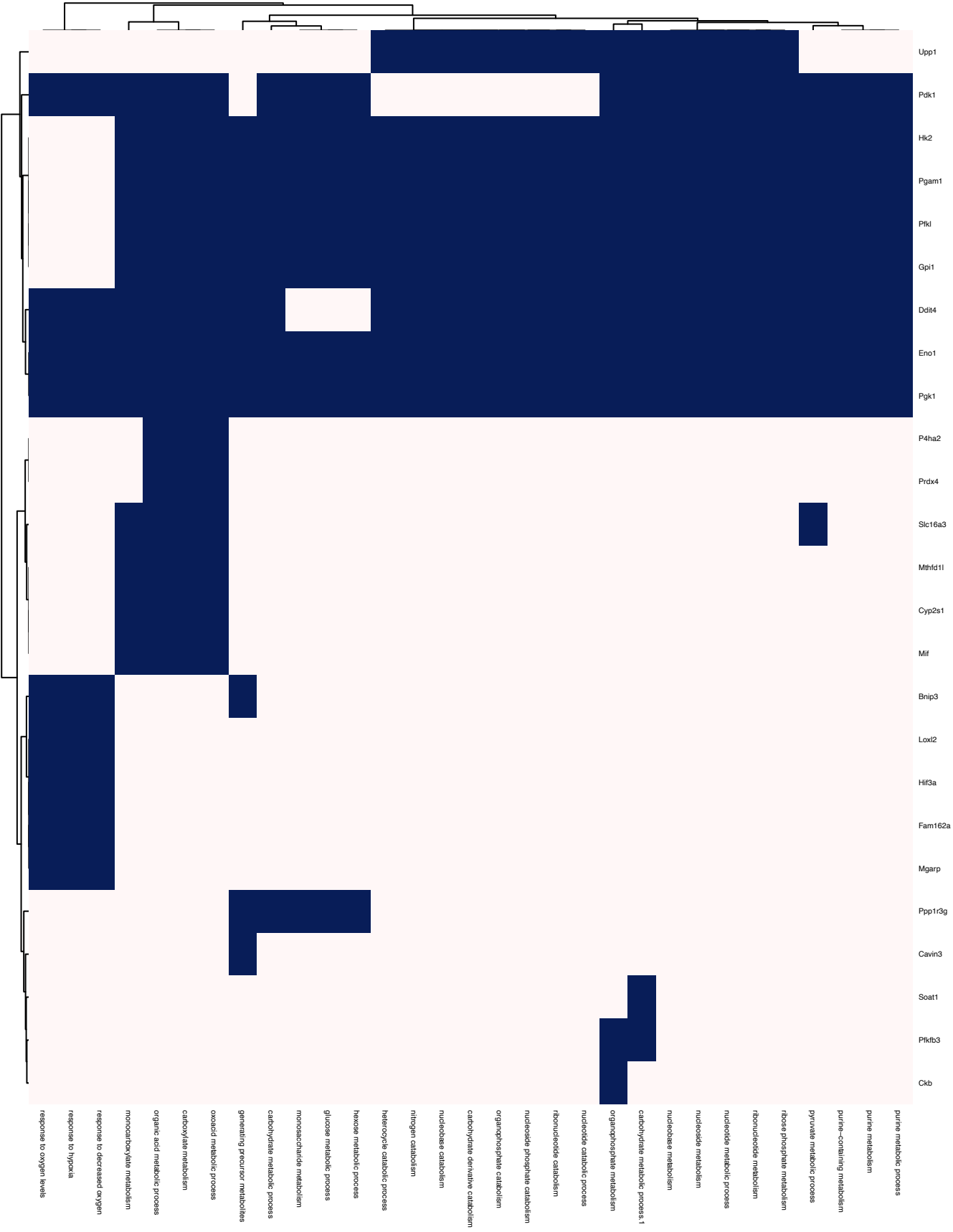
VHKO

VEKO

VHEKO

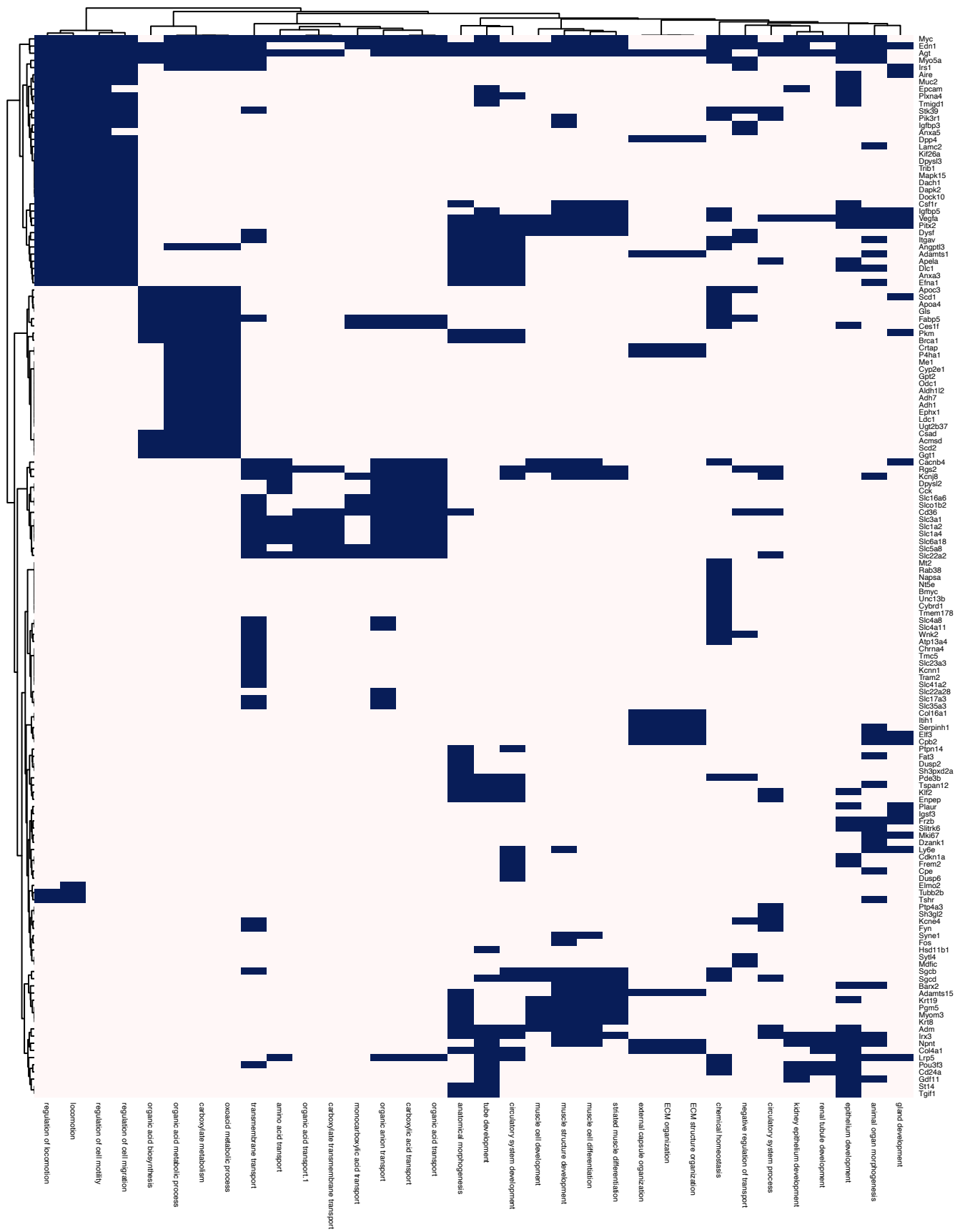
**Supplementary Fig. 6: HIF $\alpha$  isoform-specific dependent regulation of *Vhl*-dependent genes.**

Representative RNA *in situ* hybridization depicting the expression of HIF1A-specific *Pgk1* (left) and HIF2A-specific *Angptl3* (right) in renal cortex of ConKO, VKO, VHKO, VEKO, and VHEKO mice given 5x 2 mg tamoxifen and harvested late (4-12 months) following recombination. Scale bar denotes 50  $\mu$ m; 40x magnification.



**Supplementary Fig. 7: Individual HIF1A-specific upregulated genes driving over-representation in the GO terms.**

Binary heatmap depicting whether individual HIF1A-specific upregulated genes are or are not members of the indicated GO terms. Blue colored tiles represent membership of the gene in the GO term. GO terms and genes are ordered by hierarchical clustering based on the overlapping memberships of GO terms.



**Supplementary Fig. 8: Individual HIF2A-specific upregulated genes driving over-representation in the GO terms.**

Binary heatmap depicting whether individual HIF2A-specific upregulated genes are or are not members of the indicated GO terms. Blue colored tiles represent membership of the gene in the GO term. GO terms and genes are ordered by hierarchical clustering based on the overlapping memberships of GO terms.



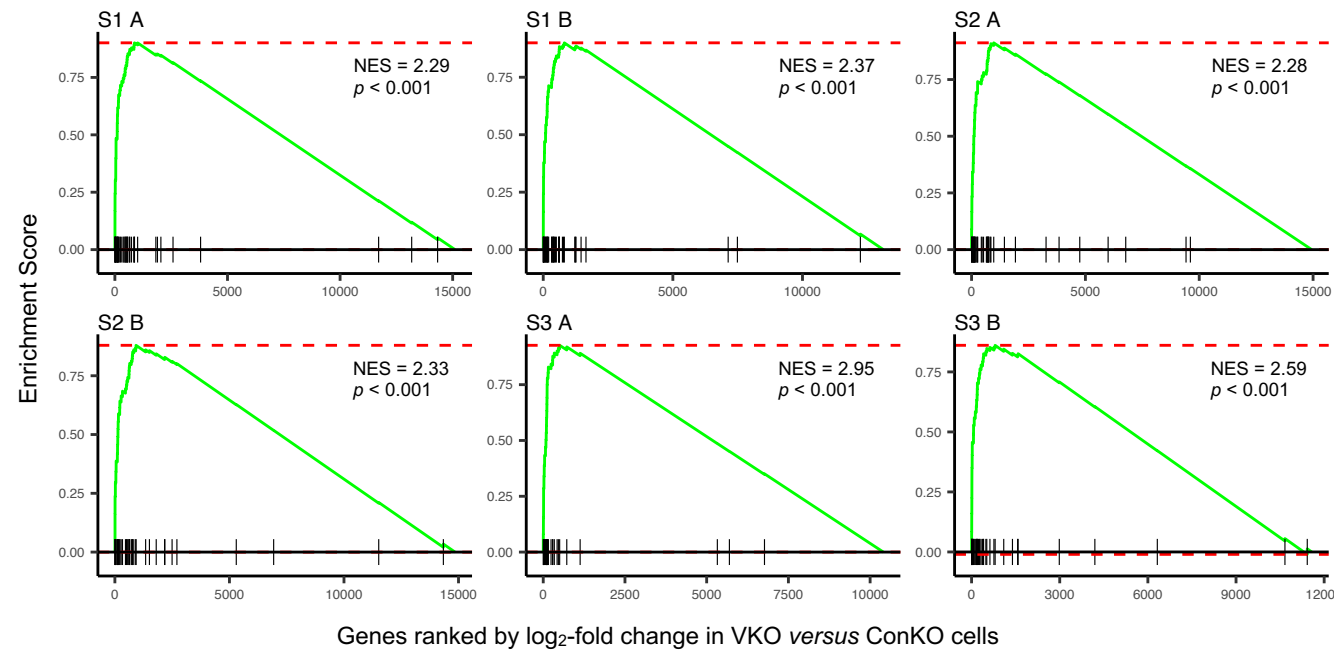
**Supplementary Fig. 9: Individual HIF2A-specific downregulated genes driving over-representation in the GO terms.**

Binary heatmap depicting whether individual HIF2A-specific downregulated genes are or are not members of the indicated GO terms. Blue colored tiles represent membership of the gene in the GO term. GO terms and genes are ordered by hierarchical clustering based on the overlapping memberships of GO terms.

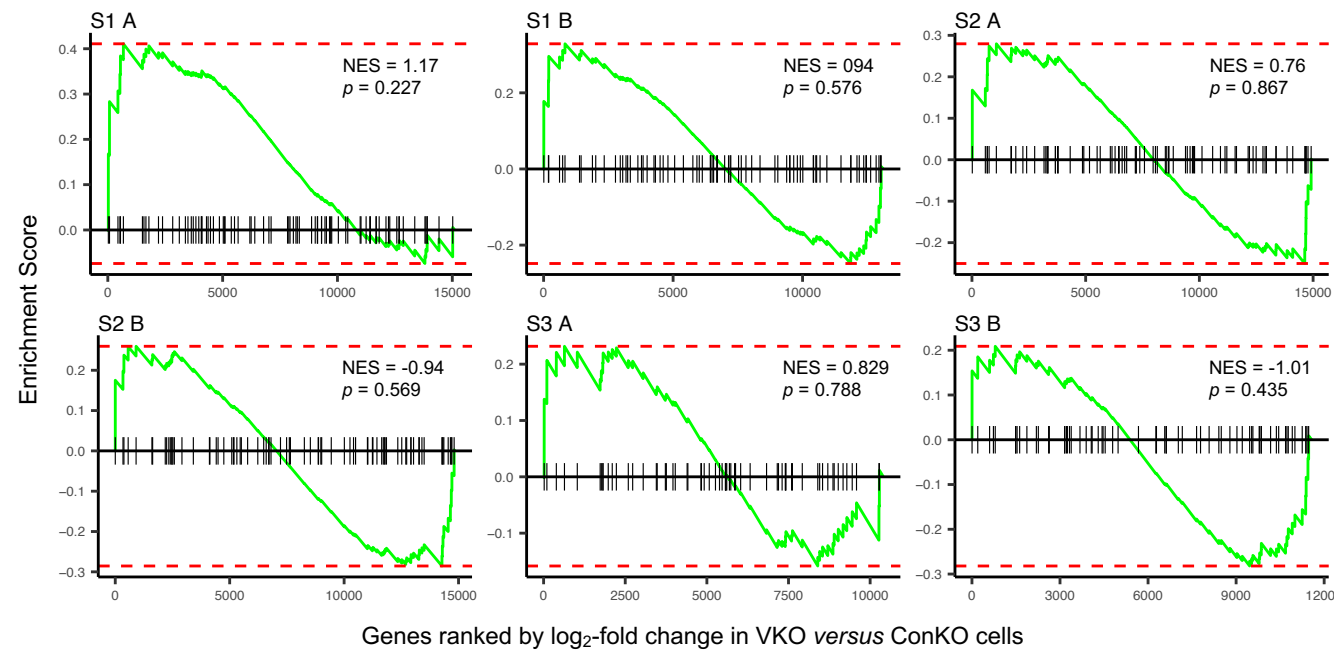


**a**

Schonenberger et al., 2016 – PT Primary Culture: HIF1A-specific genes

**b**

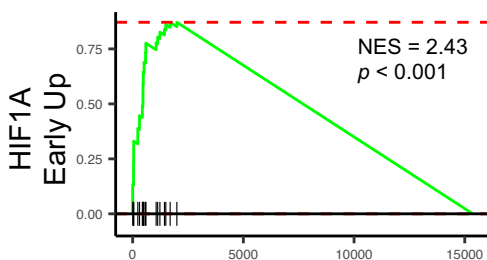
Schonenberger et al., 2016 – PT Primary Culture: HIF2A-specific genes



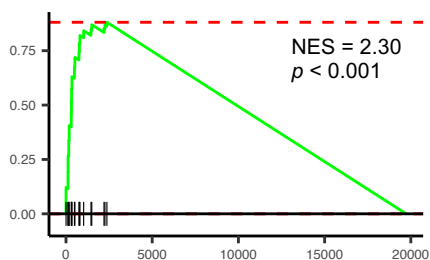
**Supplementary Fig. 10: HIF1A-dependent but not HIF2A-dependent gene regulation is conserved *in vitro* and *in vivo* model systems.**

Gene-set enrichment analysis (GSEA) on sets of **(a)** HIF1A- and **(b)** HIF2A- dependent genes, as defined in Schonenberger et al., 2016, performed on ranked lists of differentially expressed genes in VKO *versus* ConKO cells of each PT identity. NES – normalized enrichment score.

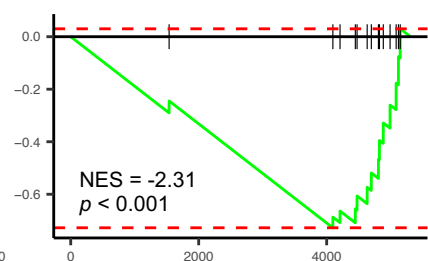
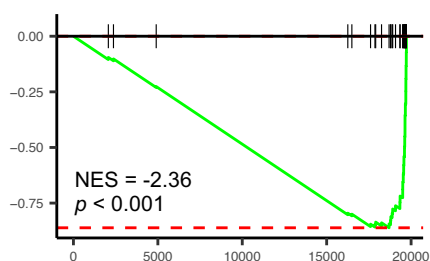
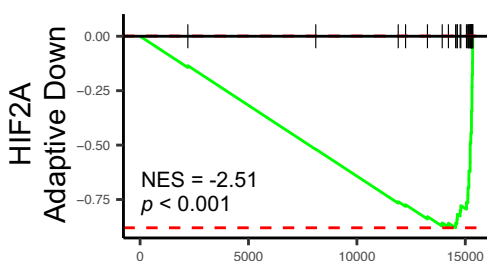
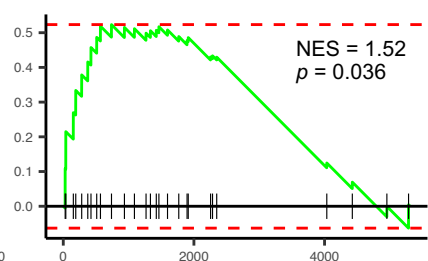
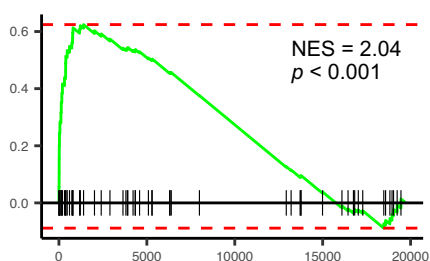
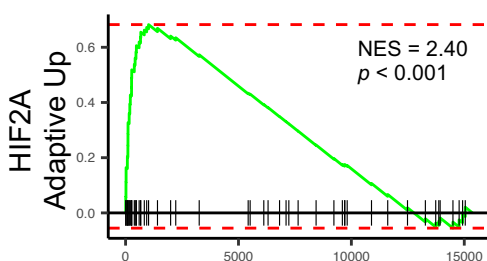
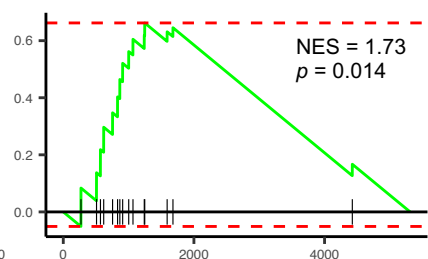
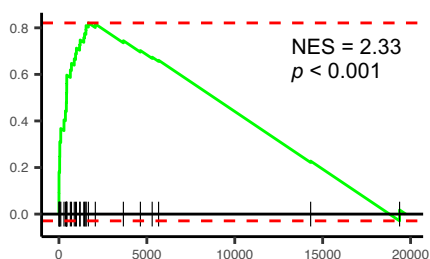
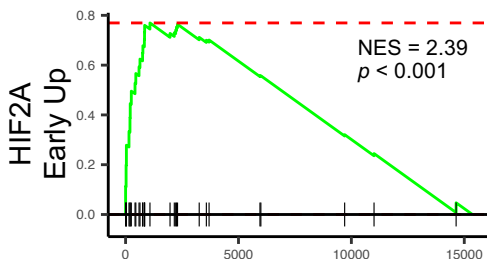
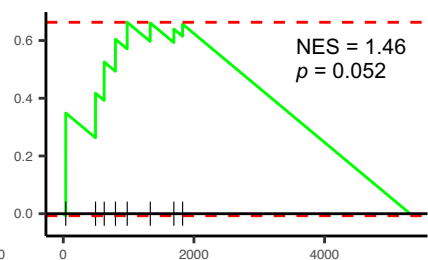
Harlander et al., 2017  
*Vhl/pRb/p53* KO ccRCC



Hoefflin et al., 2020  
*Vhl/pRb/p53* KO ccRCC

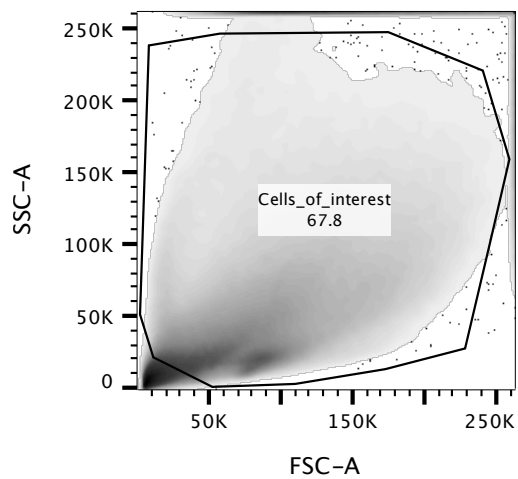
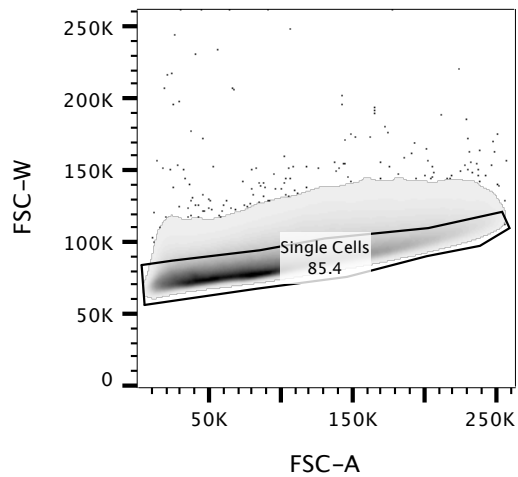
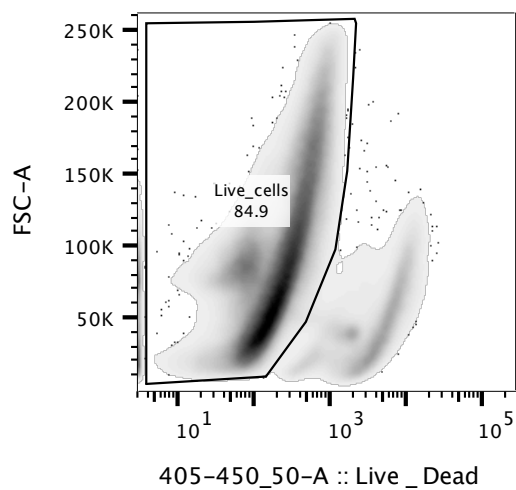
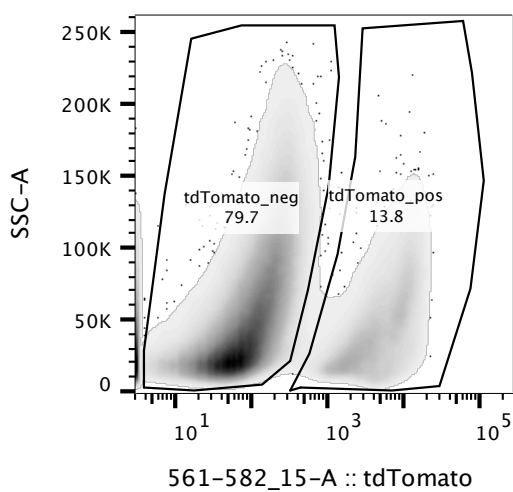


Nargund et al., 2017  
*Vhl/Pbrm1* KO ccRCC



**Supplementary Fig. 11: HIF $\alpha$ -dependent ‘early’ and ‘adaptive’ transcriptional programs in *Vhl*-null PT cells show significant associations with transcriptional programs in murine ccRCC.**

Gene set enrichment analysis (GSEA) of sets of genes upregulated early after *Vhl* inactivation in a manner dependent on HIF1A (‘HIF1A Early Up’) or HIF2A (‘HIF2A Early Up’) or regulated specifically over time in *Vhl*-null PT cells in a HIF2A-dependent manner (‘HIF2A Adaptive Up’ and ‘HIF2A Adaptive Down’). The comparisons were performed on three separate publicly-available ranked lists of differentially expressed in murine ccRCC versus normal renal cortex. NES – normalized enrichment score.

**a****b****c****d**

**Supplementary Fig. 12: Fluorescence-activated cell sorting (FACS) gating strategy used for isolation of tdTomato-positive cells.**

Representative density plots depicting the gating strategy to isolate live, single, tdTomato-positive cells from dissociated kidney cell suspension. **(a)** Cells of interest were discerned from debris by gating on Forward Scatter Area (FSC-A) *versus* Side Scatter area (SSC-A). **(b)** Single cells were discerned from doublets and aggregates by gating the cells of interest on FSC-A vs. Forward Scatter Width (FSC-W). **(c)** Live cells were identified as single cells not stained positive by DAPI, which was detected using a 405-450\_50 band/pass filter. **(d)** tdTomato-positive cells were isolated from the live, single cell population based on the positive signal detected with the 561-582\_15 band/pass filter. The percentage of cells included in each gate is indicated.